POT1 protects telomeres from a transient DNA damage response and determines how human chromosomes end

Dirk Hockemeyer[1], Agnel J Sfeir[2], Jerry W Shay[2], Woodring E Wright[2] and Titia de Lange[1,*]

[1]Laboratory for Cell Biology and Genetics, The Rockefeller University, New York, NY, USA and [2]Department of Cell Biology, University of Texas Southwestern Medical Center, Dallas, TX, USA

The hallmarks of telomere dysfunction in mammals are reduced telomeric 3′ overhangs, telomere fusions, and cell cycle arrest due to a DNA damage response. Here, we report on the phenotypes of RNAi-mediated inhibition of POT1, the single-stranded telomeric DNA-binding protein. A 10-fold reduction in POT1 protein in tumor cells induced neither telomere fusions nor cell cycle arrest. However, the 3′ overhang DNA was reduced and all telomeres elicited a transient DNA damage response in G1, indicating that extensive telomere damage can occur without cell cycle arrest or telomere fusions. RNAi to POT1 also revealed its role in generating the correct sequence at chromosome ends. The recessed 5′ end of the telomere, which normally ends on the sequence ATC-5′, was changed to a random position within the AATCCC repeat. Thus, POT1 determines the structure of the 3′ and 5′ ends of human chromosomes, and its inhibition generates a novel combination of telomere dysfunction phenotypes in which chromosome ends behave transiently as sites of DNA damage, yet remain protected from nonhomologous end-joining.

Introduction

POT1 is one of the six core components of the human telomeric protein complex (reviewed in de Lange, 2005). This complex is composed of TRF1, TRF2, TIN2, TPP1 (previously known as PIP1, PTOP, or TINT1), Rap1, and POT1, which are thought to fulfill the two main functions of telomeres: the recruitment and regulation of telomerase, and the protection of chromosome ends. Defects in telomere protection activate the DNA damage response, leading to a DNA damage signal and inappropriate DNA repair reactions at chromosome ends. The cell cycle arrest resulting from

telomere dysfunction is thought to be responsible for the finite lifespan of human cells lacking telomerase.

The current challenge is to understand how the telomeric complex protects chromosome ends from being recognized as sites of DNA damage. One approach is to define which repair and signaling pathways are repressed at natural chromosome ends by studying the events at dysfunctional telomeres. This approach has shown that chromosome ends are threatened by the nonhomologous end-joining (NHEJ) pathway (van Steensel *et al*, 1998; Bailey *et al*, 2001; Smogorzewska *et al*, 2002; Celli and de Lange, 2005). NHEJ-mediated chromosome end fusions are a prominent consequence of TRF2 inhibition and can occur when telomeres become critically short (Counter *et al*, 1992; van Steensel *et al*, 1998; Smogorzewska *et al*, 2002). In addition, dysfunctional telomeres can induce the ATM kinase and become associated with DNA damage response factors such as 53BP1, γ-H2AX, and the Mre11 complex (d'Adda di Fagagna *et al*, 2003; Takai *et al*, 2003; Herbig *et al*, 2004; Celli and de Lange, 2005).

It is generally assumed that the structure of the telomere terminus and its associated proteins is crucial for telomere function. Human telomeres contain 2–30 kb of tandem double-stranded (ds) 5′-TTAGGG-3′ repeats. The G-rich repeat strand is 50–400 nucleotides (nt) longer than the complementary 3′-AATCCC-′5 strand, resulting in a single-stranded (ss) 3′ overhang (Makarov *et al*, 1997). The final nt at the 3′ end are variable in primary human cells, but, when telomerase is active, ∼50% of the telomeres end on the sequence TAG-3′ (Sfeir *et al*, 2005). In contrast, the end of the recessed C-rich telomeric strand is defined precisely, nearly always ending with the sequence ATC-5′ (Sfeir *et al*, 2005).

The telomeric 3′ overhang can invade the duplex part of the telomere and base pair with the C-rich strand, forming a structure referred to as the t-loop. T-loops are large duplex DNA lariats observed both in purified crosslinked human telomeric DNA and in telomeric chromatin (Griffith *et al*, 1999; Nikitina and Woodcock, 2004). They may provide an architectural mechanism for the protection of telomeres from ligation by the NHEJ pathway. The NHEJ machinery is unlikely to gain access to the telomere terminus once the 3′ overhang is tucked into the duplex part of the telomere. TRF2 has been implicated in t-loop formation by *in vitro* studies (Stansel *et al*, 2001) and the induction of telomere fusions upon TRF2 loss could be explained from t-loop disruption. Furthermore, TRF2 inhibition results in degradation of the 3′ overhang by the ERCC1/XPF nt excision repair endonuclease, and this overhang loss might impair the formation of t-loops (van Steensel *et al*, 1998; Zhu *et al*, 2003).

A second interaction at the 3′ end is thought to involve POT1 (Baumann and Cech, 2001). POT1 is recruited to telomeres by TPP1 (Liu *et al*, 2004; Ye *et al*, 2004), which is a component of the TRF1 and TRF2 duplex telomeric DNA complexes (reviewed in Smogorzewska and de Lange, 2004).

Longer telomeres contain more TRF1/TRF2 complexes and also more POT1, suggesting that much of the POT1 is bound to the duplex part of the telomeric tract (Loayza and De Lange, 2003). POT1 also has two N-terminal OB folds with which it can bind 5′-(T)TAGGGTTAG-3′ either at the 3′ end or at an internal site, such as the displaced ss TTAGGG repeats at the base of the t-loop (Lei *et al*, 2004; Loayza *et al*, 2004). The crystal structure of the POT1 OB folds in complex with their recognition site suggested that POT1 might physically protect TTAGGGTTAG-3′ ends (Lei *et al*, 2004). However, only a fraction of the telomeres in primary human cells end on this sequence (Sfeir *et al*, 2005), arguing that physical capping by POT1 is not the main mode of telomere protection. Furthermore, interference with POT1 function did not show an overt telomere dysfunction phenotype (Loayza and De Lange, 2003; Liu *et al*, 2004; Ye *et al*, 2004). In these and other experiments, POT1 was found to have a key role in telomere length regulation, acting downstream of TRF1 as a negative regulator of telomere lengthening (Loayza and De Lange, 2003; Liu *et al*, 2004; Ye *et al*, 2004).

Here we show that the human *POT1* gene encodes two proteins, one of which is required for the protection of telomeres. POT1 depletion induced a unique combination of telomere dysfunction phenotypes: cells contained telomere-dysfunction-induced foci (TIFs) and had diminished amounts of ss telomeric DNA, yet they continued to proliferate and telomere fusions were not significantly induced. Furthermore, analysis of the C-rich telomeric strand identified POT1 as a factor responsible for the precise ATC-5′ ends of human chromosomes.

Results

Two forms of human POT1 generated by alternative splicing

In order to study the phenotypes of POT1 depletion induced by RNAi, we first assessed the protein products generated by the human *POT1* gene. Based on the structure of five alternatively spliced transcripts (variants V1–5), five potential polypeptides were predicted (Baumann *et al*, 2002). Antibodies raised against a peptide present in all putative variants of POT1 reacted with the 71 kDa POT1 expressed from V1 mRNA, but the polypeptides predicted to be encoded by mRNA V2, V3, and V5 were not detectable (Figure 1A; Loayza and De Lange, 2003; Daniels, Hockemeyer, and de Lange, unpublished). Instead, a POT1 polypeptide with an MW of 55 kDa (Figure 1A), referred to as POT1–55, was detected. Although POT1–55 was not a predicted product (Baumann *et al*, 2002), we noticed that the V4 mRNA, lacking exon 8, could encode a 55 kDa protein starting with an in-frame ATG in exon 9 (Figure 1A). Consistent with this, POT1–55 migrated closely to POT1ΔOB, an N-terminal truncation mutant that starts five amino acids upstream of POT1–55 (data not shown). Retroviral expression of V4 mRNA led to the overexpression of a protein that comigrated with the putative 55 kDa POT1 species (Figure 1A). In order to verify that POT1–55 was derived from V4 mRNA, we used RNAi target sites in exons shared by V1 and V4 mRNAs (exons 7 and 18), target sites in exon 8 (absent from V4), the junctions of exons 7/9 (only found in V4), and the junction of exons 7/8 (present in all POT1 mRNAs but V4) (Figure 1B and Supplementary Figure 1). The results established that the human *POT1* gene encodes two main products, the 71 kDa POT1 and the smaller POT1–55 encoded by an mRNA lacking exon 8 (Supplementary Figure 1). As POT1–55 is virtually identical to POT1ΔOB, it is expected to have the same properties: association with telomeres through protein–protein interaction, lack of DNA-binding activity *in vitro*, and the capacity to block the negative regulation of telomerase when overexpressed (Loayza and De Lange, 2003). Using an antibody raised against a peptide present in both forms of POT1, we estimate that POT1 is approximately 10-fold more abundant than POT1–55 (Figure 1B).
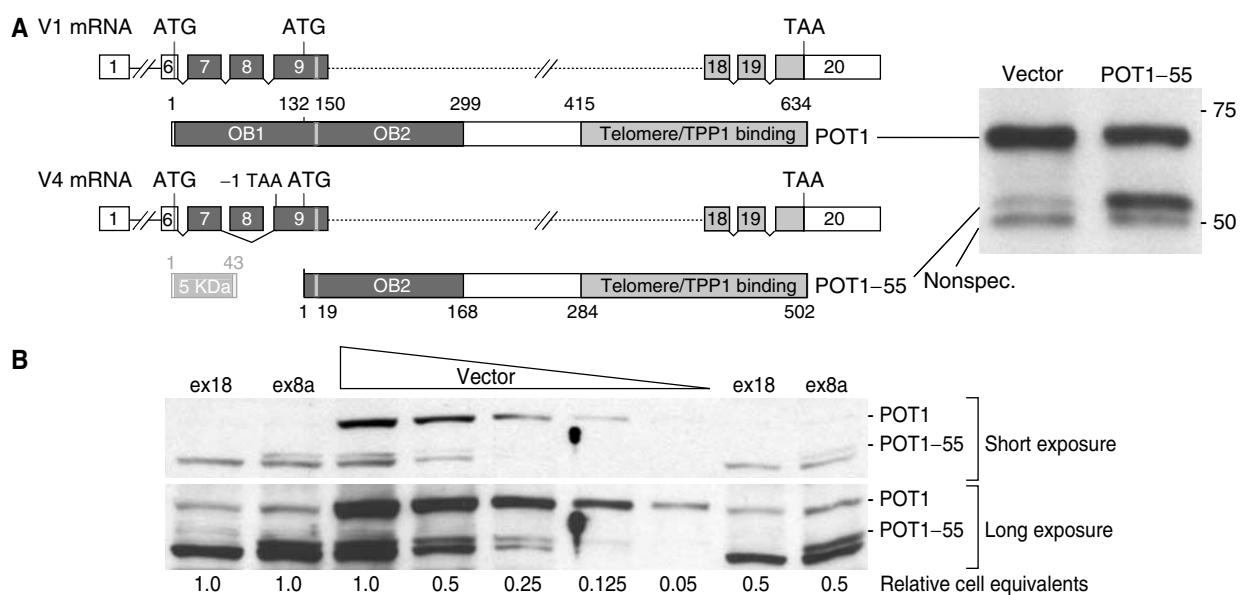
Figure 1 POT1 and POT1–55 and their depletion with RNAi. (**A**) Schematic of two POT1 mRNAs and the proteins they encode. The immunoblot to the right shows HTC75 cells infected with the pLPC vector or the same vector expressing the POT1–55 form from V4 mRNA. Dark fill: OB folds. Light fill: TPP1 interacting domain. (**B**) Quantitative immunoblot to determine the level of POT1 knockdown in HelaS3 cells. Serial dilutions of vector protein extract were compared to the indicated relative cell equivalents of ex18 and ex8a knockdown cell extracts.

TIFs without telomere fusions

The effects of lowered POT1 and POT1–55 levels on telomere protection were determined using retroviral delivery of shRNAs into primary human fibroblasts (IMR90 and BJ), fibroblasts immortalized with hTERT (BJ/hTERT), and telomerase-positive tumor cell lines (HeLa, cervical carcinoma, HTC75 fibrosarcoma, and HCT116, colon carcinoma). The RNAi reagents were named for the exons or exon junctions they target (e.g. ex18 targets exon 18; see Supplementary Figure 1). Both forms of POT1 were targeted with ex7 and ex18; ex7/8 and ex8a and b affected POT1 but not POT1–55, and ex7/9a and b partially depleted POT1–55 without affecting POT1 (Supplementary Figure 1).

Quantitative immunoblotting showed that the residual POT1 levels in HeLaS3 cells were ∼5–10% for shRNAs ex18 and ex8a (Figure 1B). Similar knockdown effects were observed in BJ fibroblasts and HCT116 cells, whereas HTC75 and HT1080 cells were found to be less efficient for RNAi (Figures 1, 5, and Supplementary Figure 3; data not shown). Western blotting analysis of synchronized HeLa cells indicated that the knockdown of POT1 was stable through the cell cycle (data not shown). Telomeric ChIP confirmed that HeLa cells expressing shRNA ex18 (targeting both forms) or ex8a (specific for POT1) had reduced levels of POT1 at telomeres (Supplementary Figure 2). The average reduction of telomeric DNA recovered in the POT1 ChIP was 6.7-fold ($n = 3$; s.d. ± 1.5-fold). There was no loss of the duplex telomeric repeats and other components of the telomeric protein complex (TRF1, TRF2, Rap1, and TIN2) remained associated with telomeric DNA (Supplementary Figure 2; see below). Thus, RNAi can remove >90% of POT1 from the telomeric complex. RNAi has obvious limitations, since there is residual POT1 expression. Information on the null phenotype of mouse POT1 will require dual deletion of the two POT1 genes in the mouse genome. Yet, POT1 RNAi is still informative not only because it allows analysis of human cells but also because partial inhibition of other human telomeric proteins has identified important hallmarks of telomere dysfunction in previous studies (van Steensel *et al*, 1998; Karlseder *et al*, 1999; Kim *et al*, 2004).

As telomere fusions are a pervasive signature of telomere dysfunction, metaphase chromosomes were examined for this defect. In HTC75 and HeLa cells, the frequency of chromosome end fusions after stable POT1 knockdown was increased less than two-fold compared to the control cultures (Figure 2A and B), resulting in approximately one telomere fusion event in 25 cells. A similar result was obtained when cells were examined after transient transfection with siRNAs directed to POT1 or when chromosome fusions were evaluated without telomeric FISH (data not shown). This frequency of chromosome end fusions was also recently reported by others for cells with similar or milder POT1 knockdown levels (Veldman *et al*, 2004; Yang *et al*, 2005). The significance of this phenotype was evaluated by comparing it to the expression of partial inhibition of TRF2 using the dominant-negative allele (TRF2$^{\Delta B \Delta M}$). Expression of this allele of TRF2 increased the frequency of telomere fusions by 10–100-fold, and fusions are observed in 50% of the cells (Figure 2B; van Steensel *et al*, 1998). Thus, in comparison to partial inhibition of TRF2, the telomere fusion phenotype of POT1 depletion is marginal.

The absence of significant telomere fusions could indicate that normal POT1 levels are not required for this aspect of telomere protection. Alternatively, POT1 could be necessary for both telomere protection and for the processing of telomeres by NHEJ. While counterintuitive, this situation is not unprecedented, as the Ku heterodimer is required for both the protection of chromosome ends and their fusion by NHEJ (Bailey *et al*, 1999). As a consequence, Ku-deficient cells have a very low number of telomere fusions even when TRF2 is absent (Celli and de Lange, unpublished). In order to test whether this scenario pertains to POT1, we asked whether POT1 shRNA lowered the frequency of telomere fusions in cells expressing TRF2$^{\Delta B \Delta M}$, the dominant-negative allele of TRF2. The results showed that POT1 depletion does not inhibit telomere fusions in this context (Figure 2B). On the contrary, POT1 depletion slightly increased the incidence of telomere fusions after TRF2 inhibition. The significance of this increase remains to be determined.

As a second index for telomere dysfunction, we analyzed the formation of TIFs in POT1 knockdown cells. Cells treated with shRNA to POT1 ex18 had significant levels of TIFs, as shown by the colocalization of 53BP1 and γ-H2AX with TRF1 (Figure 3). In asynchronous populations of BJ fibroblasts and HeLa cells, up to 40% of the cells had >10 TIFs and, in these TIF-positive cells, the majority of the TRF1 signals coincided with 53BP1 (Figure 3B and C). Telomerase expression did not affect this phenotype (Figure 3C; Wilcoxon test on the distribution of TIF frequencies in BJ and BJ/hTERT cells indicated that the difference is not statistically significant, $P = 0.3$). Synchronization of HeLa cells by double-thymidine block (Figure 3D and E) or elutriation (data not shown) showed that TIFs were particularly prominent in G1, but rare or undetectable in S and G2 cells. This is not due to a cell cycle variation in POT1 knockdown, since immunoblotting and ChIP analysis showed that the residual levels of POT1 were the same in G1, S, and G2/M (data not shown). Therefore, the transient telomere damage response indicated that normal POT1 levels were required to repress a DNA damage signal at telomeres in G1, but not in S and G2. This phenotype is different from that of TRF2 inhibition, as conditional deletion of mouse TRF2 generates TIFs in all interphase cells (Celli and de Lange, 2005) and expression of a dominant-negative allele of TRF2 in HeLa cells can generate TIFs in S and G2 phase (Takai *et al*, 2003).

Impaired proliferation of primary, but not transformed, cells

Despite the occurrence of frequent TIFs in G1, HeLa cells did not show significant growth defects after knockdown of POT1 (Figure 4A). Consistent with their unimpaired proliferation, synchronized cells did not reveal an obvious delay in the cell cycle, and the FACS profile of POT1 shRNA cells was indistinguishable for vector control cells (Figure 4B; data not shown). We considered that the lack of a cell cycle arrest might be due to selection of a subpopulation of cells that can tolerate low POT1 levels. To address this, we examined the proliferation of HeLa cells treated with siRNA, allowing the detection of immediate effects occurring in the first few days after POT1 depletion. Also, in this setting, the HeLa cells treated with POT1 siRNA behaved identically to cells treated with a control (luciferase) siRNA (Figure 4C; see for Western analysis Supplementary Figure 1B). Furthermore, no growth
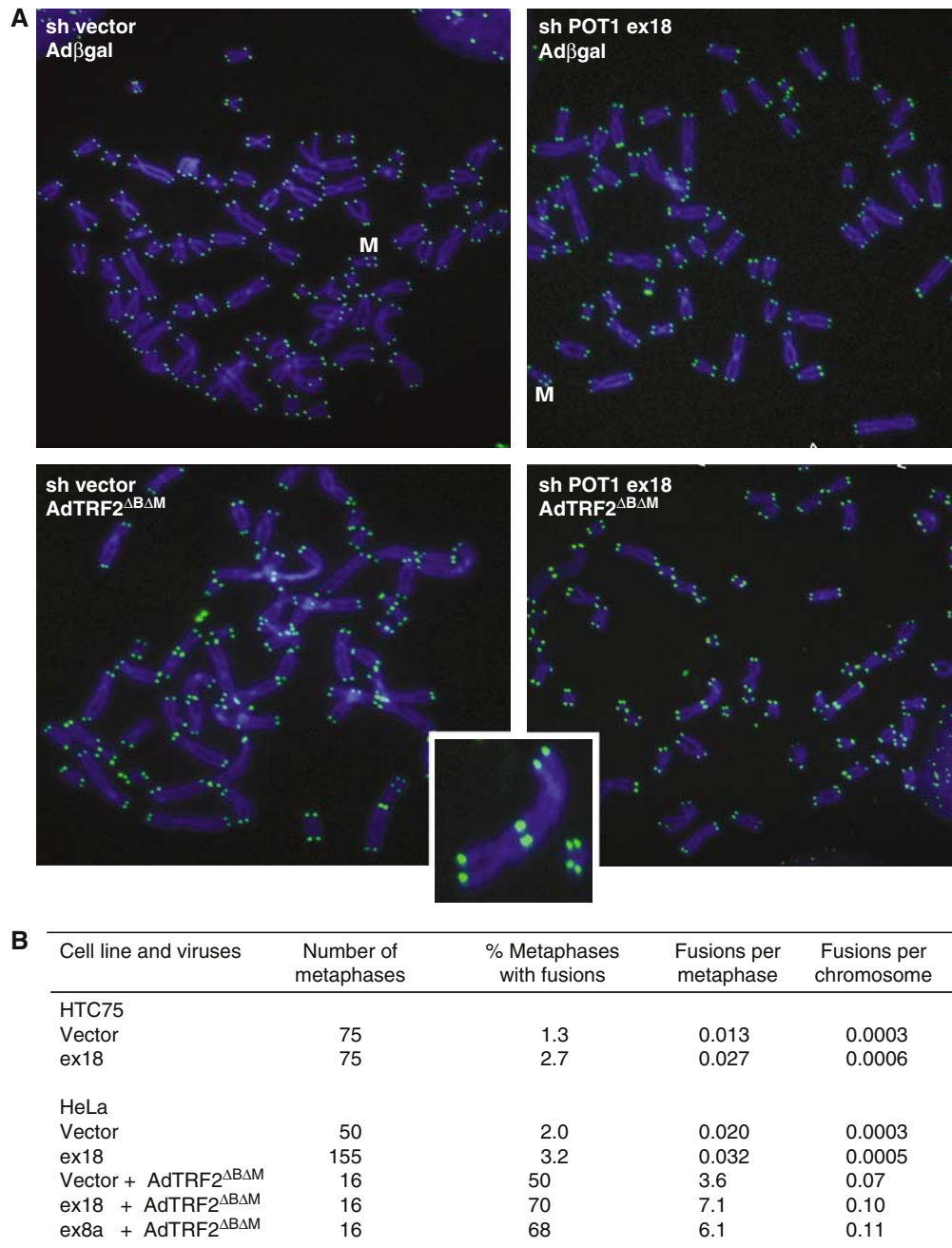
Figure 2 POT1 depletion does not induce significant levels of chromosome end fusions. (**A**) Metaphase spreads of the indicated HeLa cells with telomeric DNA detected by FISH (green). HeLa cells stably expressing the indicated shRNAs were infected with adenovirus expressing the TRF2 dominant-negative allele (AdTRF2$^{\Delta B\Delta M}$) or a control adenovirus (Adβgal), and processed for chromosome analysis after 2 days. M indicates a marker chromosome with internal TTAGGG repeats. The inset shows an enlarged image of one chromosome-type fusion from the AdTRF2$^{\Delta B\Delta M}$/POT1 shRNA panel. (**B**) Summary of the frequency of chromosome fusions in HeLa cells and HCT75 cells stably expressing POT1 shRNA and treated with the AdTRF2$^{\Delta B\Delta M}$ adenovirus to inhibit TRF2. Chromosomes were analyzed 2 days after introduction of AdTRF2$^{\Delta B\Delta M}$ and 15 days after knockdown of POT1.

Cell line and viruses	Number of metaphases	% Metaphases with fusions	Fusions per metaphase	Fusions per chromosome
HTC75				
Vector	75	1.3	0.013	0.0003
ex18	75	2.7	0.027	0.0006
HeLa				
Vector	50	2.0	0.020	0.0003
ex18	155	3.2	0.032	0.0005
Vector + AdTRF2$^{\Delta B\Delta M}$	16	50	3.6	0.07
ex18 + AdTRF2$^{\Delta B\Delta M}$	16	70	7.1	0.10
ex8a + AdTRF2$^{\Delta B\Delta M}$	16	68	6.1	0.11

defect was observed in HTC75 and HCT116 cells (data not shown). We conclude that the depletion of POT1 does not significantly affect the proliferation of these tumor cell lines, despite the presence of telomere damage detectable by the TIF assay.

In contrast to tumor cell lines, primary human fibroblasts responded to POT1 depletion with strongly reduced proliferation and induction of a senescent phenotype in a subset of the cells (Figure 4D and E). This phenotype was largely rescued

by overexpression of a POT1 cDNA with a silent mutation in the shRNA ex18 target site (Figure 4E), arguing that it is due to lack of full-length POT1 rather than reflecting a function of POT1–55. Induction of senescence was also observed for BJ fibroblasts and telomerase-positive BJ/hTERT cells (data not shown), indicating that telomerase status does not determine how cells respond to POT1 depletion. In contrast, abrogation of the p53 and p16/Rb pathways with SV40 large T improved the proliferation of cells with diminished POT1 (Figure 4F).
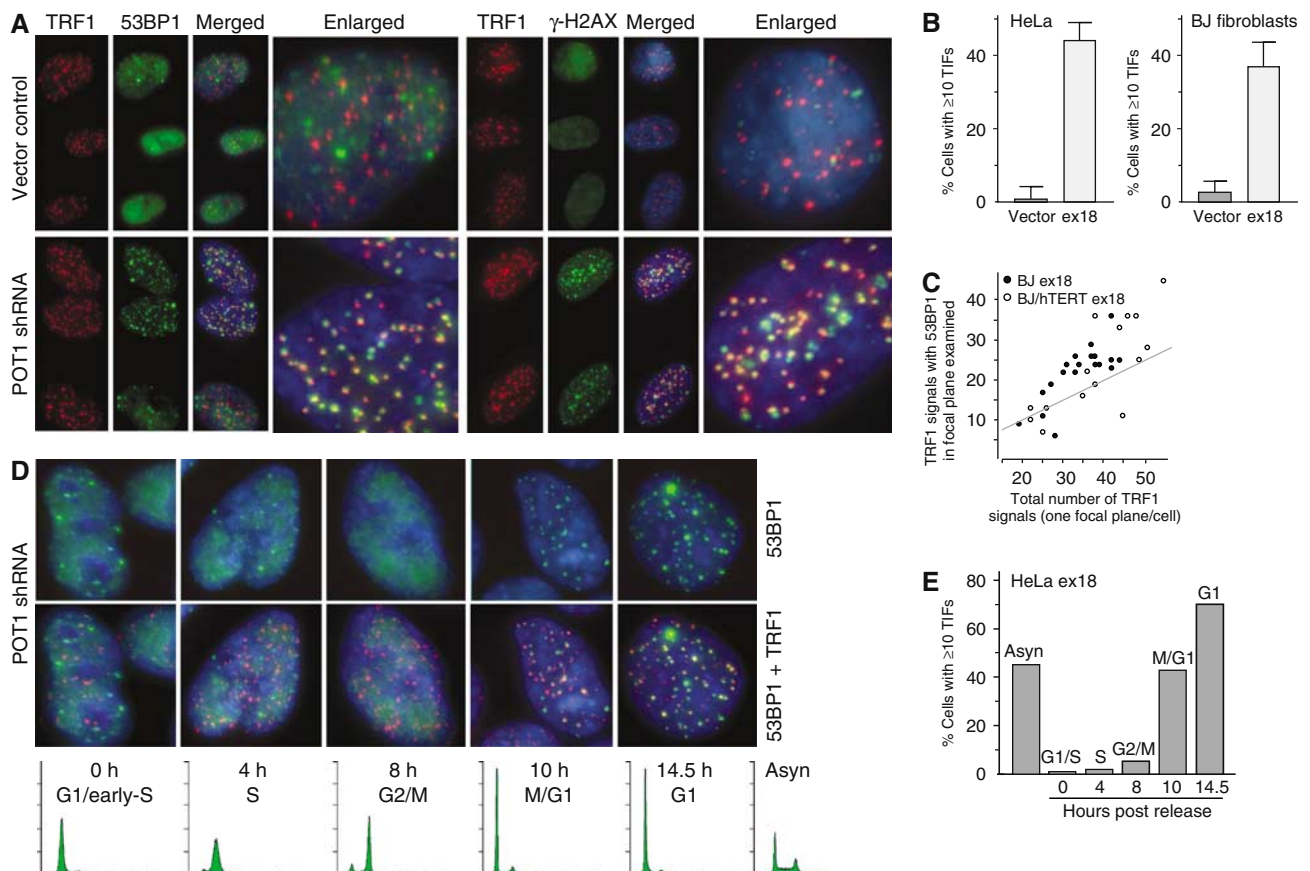
Figure 3 Transient telomere damage response upon POT1 depletion. (**A**) TIFs induced by POT1 shRNA ex18. BJ/hTERT cells were processed for TIF analysis 8 days after infection and selection of the ex18 vector or the vector control by IF for TRF1 (red) and 53BP1 (green) or γ-H2AX (green). Merged images are shown with DAPI. (**B**) Quantification of the induction of TIFs by POT1 ex18 shRNA. IF for TRF1 and 53BP1 (see (A)) was used and randomly selected groups of cells were evaluated for the number of TRF1 signals per cell that contained a 53BP1 signal. The bars show the percentage of cells containing 10 or more TIFs. (**C**) The majority of the telomeres in TIF-positive cells colocalize with 53BP1. TIF-positive BJ (●) and BJ/hTERT (○) cells were selected and imaged using deconvolution software. Each point in the graph represents one TIF-positive cell and shows the number of TRF1 signals plotted versus the number of TRF1 signals containing 53BP1. Points above the line represent cells in which more than 50% of the TRF1 signals contained 53BP1. (**D**) Transient TIFs in G1. HeLa cells expressing POT1 shRNA ex18 or vector control were released from double-thymidine block and processed for IF at the indicated time points. FACS profiles are shown below the IF images. Top: 53BP1 signal (green) merged with DAPI (blue). Bottom: 53BP1, TRF1 (red), and DAPI signals merged. (**E**) Quantification of cell cycle dependence of TIF-positive cells. Quantification as in (B), using the cells shown in (D).

However, SV40LT-expressing cells still had a slightly diminished growth rate when POT1 was inhibited (Figure 4F).

Protection of telomeric overhangs by POT1, but not POT1–55

Whereas fission yeast that lack POT1 undergo an immediate loss of all telomeric DNA (Baumann and Cech, 2001), the duplex part of human telomeres persisted after depletion of POT1 (Figure 5; data not shown). However, a quantitative assay for the amount of ss TTAGGG repeat DNA showed that POT1 inhibition affected the maintenance of the 3′ telomeric overhang (Figure 5). The ratio of ss to ds TTAGGG repeats of IMR90 telomeres (measured by an in-gel hybridization assay) was reduced by 30–40% within a week after introduction of three different shRNAs (Figure 5A and B). Similar reduction of the overhang signal was observed upon POT1 knockdown in BJ and BJ/hTERT cells, showing that the effect is not counteracted by telomerase (Figure 5C–H). The loss of overhang signal was also observed in HeLa and HCT116 tumor cell lines. In these settings, overhang reduction was a stable

phenotype that persisted for at least 40 PD (Supplementary Figure 3). Ex7/9 shRNAs, which did not affect POT1 and only mildly reduced POT1–55, did not alter the ss TTAGGG signal (Figure 5C–H). The overhang phenotype could be rescued by coexpression of a version of POT1 resistant to shRNA ex18 (Supplementary Figure 3). Since the rescuing construct did not express POT1–55, POT1 was sufficient to protect the overhangs. Furthermore, one of the shRNAs (ex8a) that resulted in overhang loss did not affect POT1–55 (Figure 5A), consistent with the phenotype being due to diminished full-length POT1. Nevertheless, it cannot be excluded that POT1–55 also plays a role in the regulation of telomere overhang formation or overhang protection.

POT1 determines the last nt of human chromosomes

The 5′ end of human chromosomes is remarkably specific, ending more than 80% of the time with the sequence ATC-5′ (Sfeir *et al*, 2005). To test whether POT1 is required to define this precise ending, we used the recently developed ligation-mediated PCR assay. In this assay, oligonucleotides
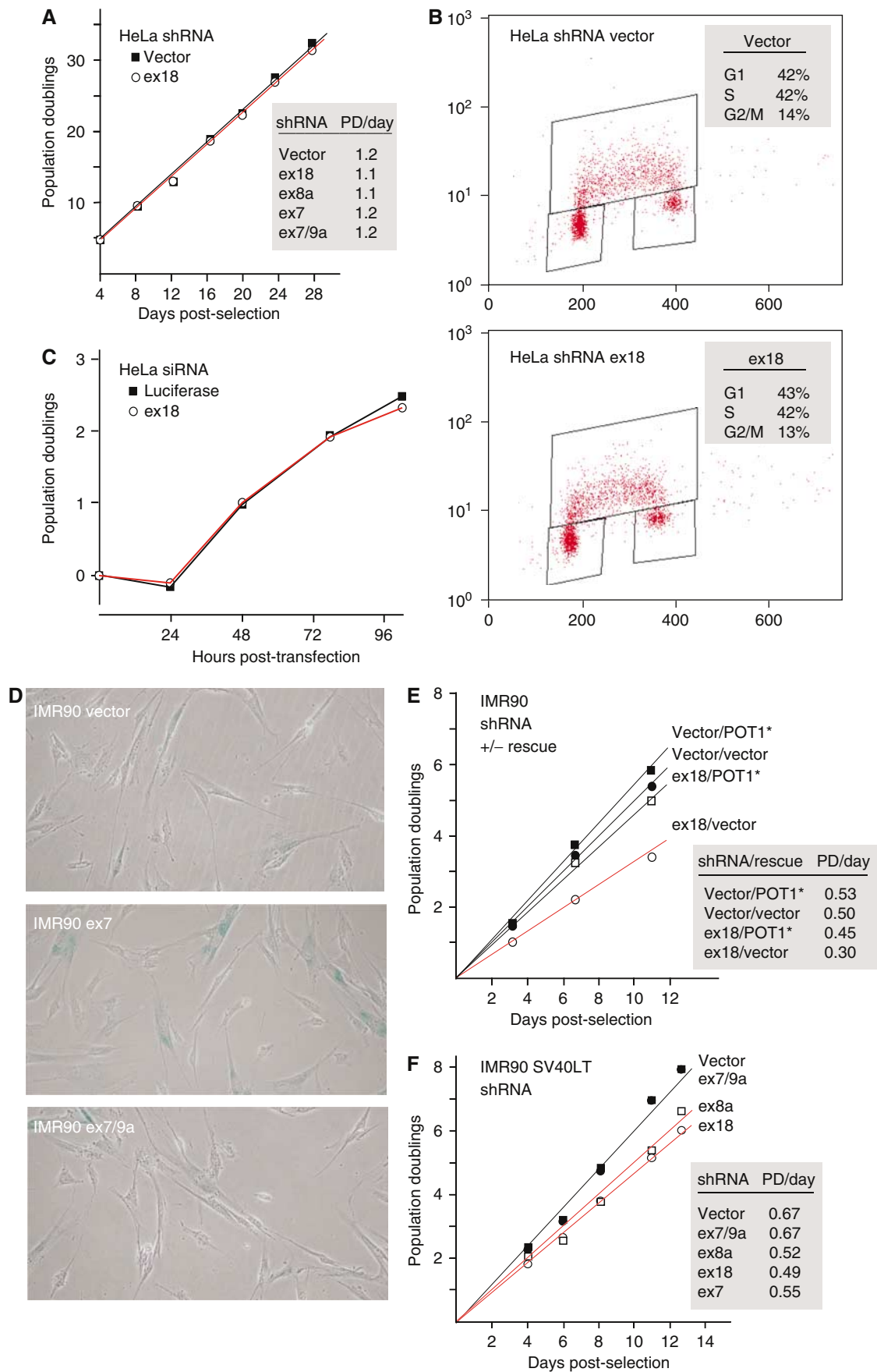
(5′ telorettes) representing the six different phases within the 3′-AATCCC-5′ telomeric repeat sequence are ligated to the 5′ end of the chromosome, using the telomeric overhang as an annealing platform (Figure 6A). The product is amplified with two nontelomeric primers, one that anneals to a sequence common to the 5′ telorettes and the other that anneals to a subtelomeric site in the pseudo-autosomal region of the X and Y chromosomes. Prior to amplification, the DNA is diluted to the point where individual molecules are amplified to give discrete bands, so that the number of bands is proportional to the number of ligated telomeres. This assay previously established that both ends (the lagging and the leading end) of each human chromosomes have the same 5′ terminal sequence and that this sequence is not influenced by telomerase activity (Sfeir *et al*, 2005). The 5′ telorette assay showed the expected predominance of the sequence ATC-5′ in vector control HeLa cells (Figure 6B). Depletion of POT1 with two different shRNAs had a striking effect, leading to nearly random ends representing all six possible terminal nt (Figure 6C and D). Similarly, BJ cells lost their prevalence for ATC-5′ ends upon knockdown of POT1 (Figure 6E; data not shown). BJ fibroblasts showed some residual predominance of ATC-5′ ends, most likely because they were analyzed within a week after POT1 depletion. A POT1 cDNA mutated to create resistance to the shRNA reverted the structure of the 5′ end to its normal ATC-5′ setting (Figure 6F), indicating that POT1 alone, in the absence of POT1–55, is sufficient to restore the 5′ end sequence. We conclude that POT1 is required for the precise determination of the sequence at the 5′ ends of human chromosomes.

Discussion

As anticipated from the function of fungal POT1-like proteins, human POT1 is required for telomere integrity. RNAi to human POT1 leads to an aberrant structure of the telomere terminus and the induction of TIFs. Unexpectedly, POT1 inhibition did not result in telomere fusions and cells with prominent TIFs continued to proliferate unimpeded. When TRF2 is inhibited, telomeres not only have altered telomere termini and TIFs, but also undergo fusions in G1 and G2 and induce cell cycle arrest. Therefore, the deprotected telomeres resulting from POT1 inhibition are distinct from those lacking sufficient TRF2. The difference is not due to fewer telomeres being affected by POT1 RNAi, because the structural and functional defects occurred at many more telomeres; yet, cells proliferated normally and chromosome ends remained protected from the NHEJ pathway. We conclude therefore that telomeres can escape NHEJ despite having an aberrant structure that elicits the DNA damage response. In addition, the POT1 RNAi data indicate that TIFs are not necessarily harbingers of impending cell cycle arrest. The analysis of synchronized cells showed that these TIFs are present every

time a cell exits mitosis. This is a stable phenotype in HeLa cells, arguing against the detrimental effects of TIFs on cell proliferation, and there is no indication that the TIFs induce a cell cycle arrest in G1. One possibility is that the type of telomere damage induced by lowered POT1 levels is repaired in G1 before a cell cycle arrest is induced.
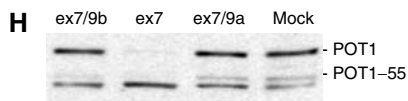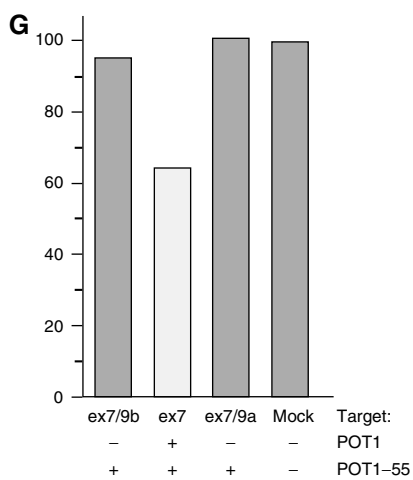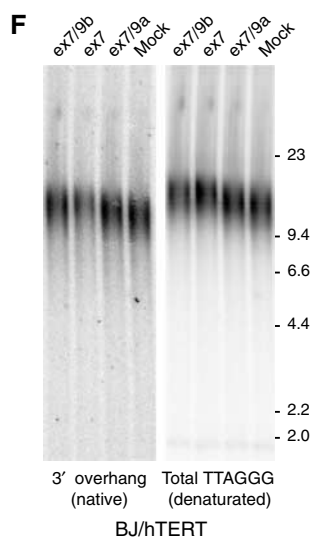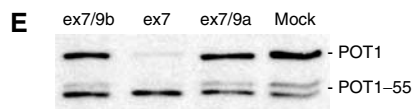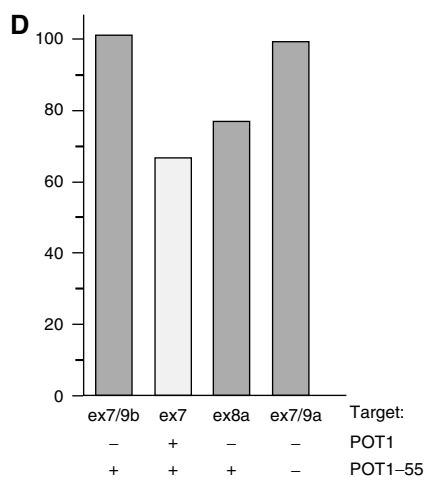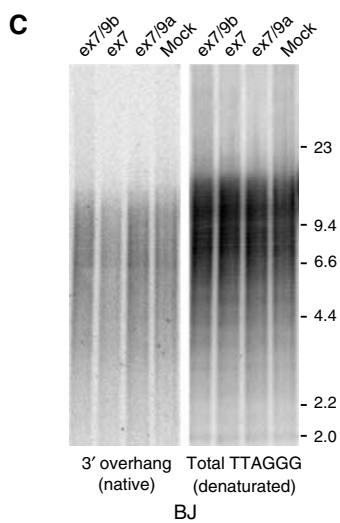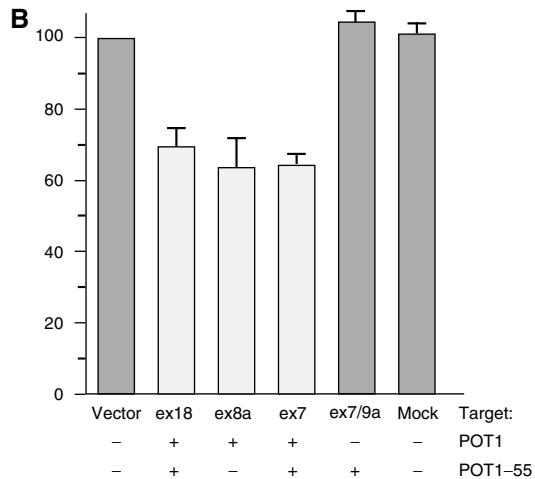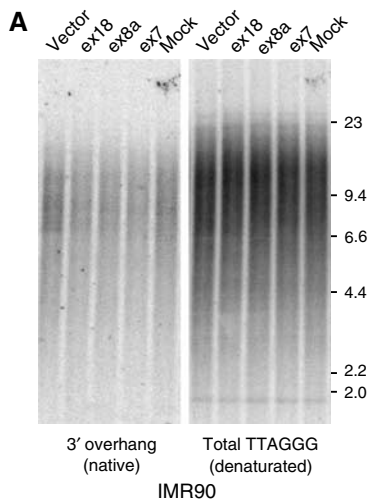
Unraveling these distinct aspects of telomere protection illuminated by inhibition of TRF2 and POT1 is pertinent to the question of how telomere attrition induces senescence in primary human cells. Although the reduced presence of TRF2 on short telomeres can explain many aspects of critically shortened telomeres, concomitant reduction in POT1 may well contribute to the behavior of cells as they approach the end of their replicative lifespan. In this regard, the partial inhibition of POT1 achieved with RNAi may be more informative than the null phenotype.

Definition of the 5′ end

Our data show that normal POT1 levels determine the ultimate 5′ end of human chromosomes. When POT1 is diminished, the 5′ ends terminate at all positions in the 3′-AATCCC-5′ repeat strand; when POT1 is fully functional, human chromosomes end with ATC-5′. How does POT1 set the end? Two general models can be envisaged. In one, POT1 recruits a nuclease that specifically cleaves the C-strand at the 3′-AATC^CC-5′ position. Nuclease trimming of the C-strand has been invoked to explain the formation of 3′ overhangs and the high shortening rate of human telomeres (Makarov *et al*, 1997). Perhaps the diminished recruitment of a C-strand nuclease in cells with diminished POT1 results in incomplete processing of telomeres that have just been replicated. This could explain both the lack of specific C-strand ends and the diminished amount of ss TTAGGG repeats seen upon POT1 shRNA. In a variation of this model, POT1 does not recruit the nuclease, but stimulates it. POT1 could act similarly to another OB-fold ss DNA-binding protein, RPA, which directs the nuclease ERCC1/XPF in NER (de Laat *et al*, 1998).

A second possibility is that POT1 protects the sequence ATC-5′, but not other ends, from nucleolytic attack. In this model, the nuclease that generates telomeric overhangs need not be specific for the sequence ATC-5′ and degradation would continue until an end is generated that POT1 can protect. The ATC end is very close to the first POT1 recognition site (5′-(T)TAGGGTTAG-3′) in the 3′ overhang, perhaps allowing protection. The tethering of POT1 to the TRF1(2)/TIN2/TPP1 complex, lodged on its nearby duplex 5′-YTAGG GTTR-3′ half-sites (Bianchi *et al*, 1999), could also contribute to the protection of the 5′ end. Biochemical and structural studies may be able to clarify these issues. The idea that POT1 acts to protect the end from further nuclease attack is attractive because budding yeast Cdc13, a telomeric protein of substantially similar structure, protects the C-rich strand of yeast telomeres from degradation (Garvik *et al*, 1995).

Figure 4 Differential effect of POT1 shRNA on proliferation of primary and transformed cells. (**A**) Graph showing growth curves of HeLa cells with and without POT1 shRNA. The inset shows the growth rate (PD/day) of these and additional HeLa cells with lowered POT1 level. (**B**) Graph showing proliferation of HeLa cells transfected with POT1 siRNA or control siRNA. (**C**) FACS profiles of BrdU-labeled HeLa cells infected with the indicated shRNA viruses. Insets show the % cells in G1, S, and G2/M. (**D**) Phase-contrast microscopic images of IMR90 cells 7 days after infection and selection with the indicated shRNA viruses stained for SA-β-galactosidase activity (Dimri *et al*, 1995) for 10 h. (**E**) Graph showing the effect of POT1 shRNA ex18 on the proliferation of IMR90 cells. The inset shows the growth rates (PD/day) in cells infected with the indicated shRNAs and a vector expressing a POT1 cDNA resistant to ex18 shRNA (POT1*). (**F**) Graph showing the effect of POT1 shRNAs on IMR90 cells transformed by introduction of SV40 large T antigen (pBabeNeoLT). The inset lists the growth rate of the cells.

A

3′ overhang (native) | Total TTAGGG (denatured)

Vector | ex18 | ex8a | ex7 | Mock | Vector | ex18 | ex8a | ex7 | Mock

23
9.4
6.6
4.4
2.2
2.0

IMR90

B

Target:						
Vector	ex18	ex8a	ex7	ex7/9a	Mock	
−	+	+	+	−	−	POT1
−	+	−	+	+	−	POT1–55

C

ex7/9b | ex7 | ex7/9a | Mock | ex7/9b | ex7 | ex7/9a | Mock

23
9.4
6.6
4.4
2.2
2.0

3′ overhang (native) | Total TTAGGG (denatured)

BJ

D

Target:			
ex7/9b	ex7	ex8a	ex7/9a
−	+	−	−	POT1
+	+	+	−	POT1–55

E

ex7/9b | ex7 | ex7/9a | Mock

- POT1
- POT1–55

F

ex7/9b | ex7 | ex7/9a | Mock | ex7/9b | ex7 | ex7/9a | Mock

23
9.4
6.6
4.4
2.2
2.0

3′ overhang (native) | Total TTAGGG (denatured)

BJ/hTERT

G

Target:			
ex7/9b	ex7	ex7/9a	Mock
−	+	−	−	POT1
+	+	+	−	POT1–55

H

ex7/9b | ex7 | ex7/9a | Mock

- POT1
- POT1–55

Furthermore, in *pot1*-fission yeast, all telomeric DNA, including the C-rich strand, disappears rapidly (Baumann and Cech, 2001). Although human cells treated with POT1 shRNA does not show a similar dramatic loss of the C-rich strand, it will be interesting to determine whether more extensive degradation of the C-rich strand will take place in POT1 null cells.

A transient postmitotic telomere damage signal

Cells with diminished POT1 accumulate γ-H2AX and 53BP1 at telomeres, indicating the activation of a DNA damage response at natural chromosome ends. This response was observed in cells entering G1 and had disappeared by the time cells entered S phase. The transient nature of this signal might explain why cells do not arrest upon induction of this form of telomere damage. Why does the telomere damage signal disappear? We favor the possibility that the DNA damage signal is extinguished by a process that restores the protected state of telomeres. One possibility is that POT1 is normally required to re-establish the fully protected state during or after mitosis and that the process is delayed or slow when POT1 levels are low. It is tempting to link the transient DNA damage response to the defect in the structure of the telomere termini. If POT1 generates the correct 3′ overhang by recruiting or activating a specific nuclease that leaves ATC-5′ ends, a DNA damage response could ensue as long as the termini have insufficient or no 3′ overhang. Early in G1, other nucleases, possibly stimulated by the DNA damage response, may also be able to generate a 3′ overhang ensuring telomere protection. These nucleases would leave the telomeres with a 3′ overhang of different length and with 5′ ends with an altered sequence. This process may be slow, inaccurate, and unregulated, but eventually could extinguish the telomere damage signal, allowing cells to progress into S phase.

Materials and methods

Cell culture, immunoblotting, telomere overhang assays, and ChIP were performed as described in detail by Ye *et al* (2004) and Loayza and de Lange (2003). All immunoblots for POT1 and POT1–55 were performed with an affinity-purified antipeptide antibody (#978) as described previously (Loayza and De Lange, 2003).

RNAi

ds siRNA was generated to target human POT1 or luciferase and purchased from Dharmacon. HeLa cells were transfected using Oligofectamine (Invitrogen) using a protocol supplied by the manufacturer. Specifically, 2.5×10^5 cells were inoculated to a 6-cm culture dish, and, after 16–24 h, were subjected to two sequential transfections separated by a 24-h interval. Protein for immunoblots was extracted after 48 h. POT1 levels were stably reduced using shRNAs expressed from the pSUPERIOR retroviral vector (OligoEngine). Retroviruses were produced in amphotrophic Phoenix cells and used to infect cells three times, followed by puromycin selection. HTC75 cells were grown in the presence of doxycyclin (0.250 mg/l). The luciferase target was 5′-CGTACGCG

GAATACTTCGA-3′ (Dharmacon). The target sites in POT1 were as follows:

Ex7:   5′-GGGTGGTACAATTGTCAAT-3′;
Ex7/8:   5′-GGAACTGATTATTGCTCAG-3′;
Ex7/9a: 5′-GGAACTGATTCAAGTATAT-3′;
Ex7/9b: 5′-CAAAGGAACTGATTCAAGT-3′;
Ex8a: 5′-GATATTGTTCGCTTTCACA-3′;
Ex8b: 5′-GCCCTTCCAATAATTTATA-3′;
Ex18:   5′-GTACTAGAAGCCTATCTCA-3′.

Indirect immunofluorescence (IF)

Cells were grown on glass coverslips, fixed for 10 min at room temperature (RT) with PBS containing 2% paraformaldehyde, and permeabilized for 10 min in PBS containing 0.5% Nonidet P-40. Nonspecific interactions were blocked by incubation for 30 min in PBS with 0.2% coldwater fish gelatin and 0.5% BSA (PBG). Thereafter, cells were incubated with primary antibody for 2 h at RT. Cells were washed three times for 5 min using PBG and incubated with rhodamine- or fluorescein-conjugated secondary antibodies in PBG (Jackson Laboratory, Bar Harbor, Maine 04609, USA). Antibodies used were as follows: TRF1, 371; 53BP1, MAb53BP1 (generously provided by T Halazonetis, The Wistar Institute, Philadelphia, PA); and γ-H2AX, Upstate, clone JBW301.

For each of the primary antibodies used in dual IF, bleed-through controls were performed by leaving out one of the primary antibodies. Images were obtained using a Zeiss Axioplan2 microscope and processed using Openlab software.

POT1 expression constructs

POT1–55 was cloned into the pLPC retroviral vector by PCR using POT1 variant 4 mRNA (EST Id aa66fo8.s1). This construct retained the Kozak sequence and the first POT1 ATG in exon 6. POT1* was generated by PCR mutagenesis of POT1 cDNA and expressed from pBabeNeo expression vector. The silent change was from position +1660 to 1678 to generate the sequence GTACTAGAAGCTTACTT-GA, conferring resistance to ex18 shRNA. pBabeSV40Tag was a gift from G Hannon.

Expression of TRF2$^{\Delta B \Delta M}$ and analysis of metaphase chromosomes

HeLa cells (2×10^6) were infected in suspension with adenovirus at 20 pfu/cell (Karlseder *et al*, 1999). The medium was changed 12 h later, and at 48 h post-infection the cells were treated with demecolcine (100 ng/ml; Sigma) for 1 h. Cells were harvested and prepared for metaphase spreads and FISH analysis as described previously (van Steensel *et al*, 1998; Smogorzewska *et al*, 2002).

Synchronization of HeLa cells

HeLa cells (1×10^6) were plated on coverslips in a 10 cm culture dish and treated with 2 mM thymidine 24 h later. After 14 h, cells were washed three times with prewarmed PBS and provided with fresh medium for 11 h before adding 2 mM final concentration of thymidine. After 14 h, cells were washed with prewarmed PBS and again provided with fresh medium. Cells were fixed at the indicated time points for IF staining using 2% formaldehyde in PBS, or in cold 70% ethanol for FACS analysis.

Cell cycle analysis and BrdU incorporation

HeLa 1.2.11 cells (1×10^6) were incubated for 30 min in culture medium containing 10 μM BrdU. Cells were harvested, washed twice with PBS containing 1% BSA, and fixed in cold 70% ethanol. DNA was denatured with 2 N HCl/0.5% Triton X-100 for 30 min, neutralized with 0.1 M sodium tetraborate (pH 8.5), and resuspended in 70% ethanol. Cells were recovered by centrifugation,

Figure 5 POT1 is required for the maintenance of the 3′ overhang. (**A, C, F**) In-gel assay for ss TTAGGG repeats with the indicated cell lines expressing the indicated shRNAs. DNA was isolated 7–10 days post-infection, cut with *Mbo*I and *Alu*I and processed by in-gel hybridization to a (CCCTAA)4 probe to detect ss TTAGGG repeats (left panels). The DNA was subsequently denatured *in situ* and rehybridized to the probe to detect the total TTAGGG repeat signal (right panels). (**B, D, G**) Bar graphs representing quantified overhang signals. Overhang signals in each lane were normalized to the total TTAGGG signal. The values are expressed relative to the value obtained with mock or vector (B) infected cells. The values in (B) represent averages of three experiments (SDs indicated). Below the bargraph, + and − indicate whether the shRNA targets POT1 and/or POT1–55. (**E, H**) Immunoblots of POT1 and POT1–55 levels in BJ (E) and BJ/hTERT (H) cells infected with retroviruses expressing the indicated shRNAs.
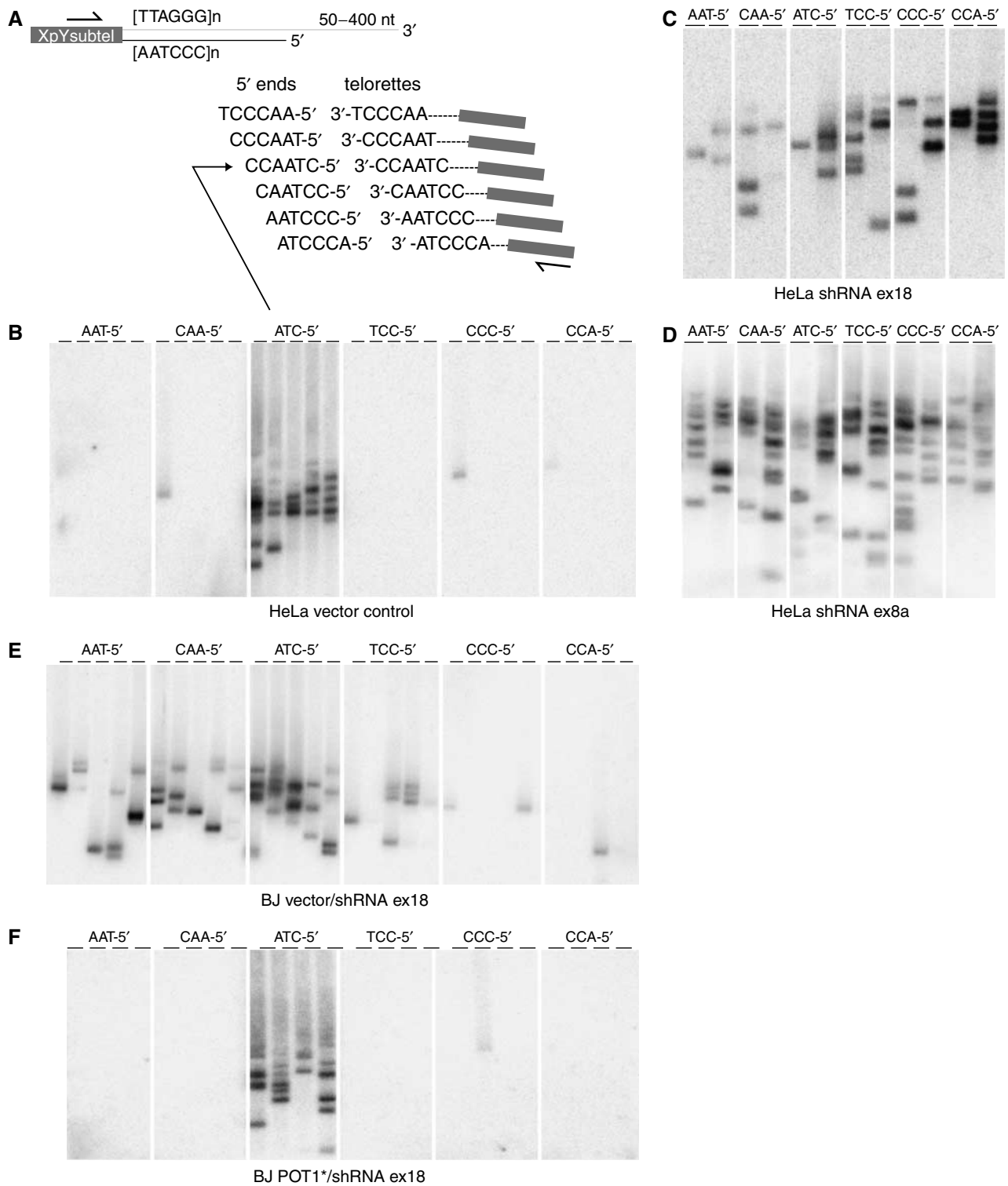
Figure 6 POT1 determines the sequence at the 5′ end of human chromosomes. (**A**) Schematic of the ends of human chromosomes and the 5′ telorette assay. The six telorettes and the 5′ ends to which they can ligate are shown. PCR primers used for amplification are shown schematically. (**B–F**) Products of the 5′ telorette assay using the indicated cell lines. Each telorette was used for 2–5 independent assays and the products were run in separate lanes. The sequences of the 5′ end detected with each telorette is shown above the groups of lanes. POT1* is a vector expressing full-length POT1 mutated to create resistance to the ex18 target site. The MWs of the detected products range from 1 to 8 kb.

resuspended in 100 μl of PBS with 0.5% Tween-20/1% BSA and 20 μl anti-BrdU antibody (Becton Dickson), and incubated at RT for 30 min. Cells were washed with PBS/0.5% Tween-20/1% BSA and resuspended in PBS/BSA containing 5 μg/ml propidium iodide. Cells were analyzed using a FacscaliburII flow cytometer and the program Cellquest.

In-gel G-overhang assay

In-gel G-overhang assay was performed essentially as described by Hemann and Greider (1999). Following electrophoresis, gels were dried down at 40°C and prehybridized at 50°C for 1 h in Church mix (0.5 M Na_2HPO_4 (pH 7.2), 1 mM EDTA, 7% SDS, and 1% BSA), followed by hybridization at 50°C overnight with an end-labeled

(CCCTAA)4 oligonucleotide. After hybridization, gels were washed three times with $4 \times$ SSC for 30 min and once with $4 \times$ SSC/0.1% SDS. Gels were exposed to PhosphoImager screens. Following G-overhang assay, gels were alkali denatured (0.5 M NaOH and 1.5 M NaCl), neutralized (3 M NaCl and 0.5 M Tris–HCl (pH 7.0)), rinsed with H$_2$O, and reprobed with the (CCCTAA)4 oligonucleotide at 55°C and then processed as previously. To determine the relative overhang signal, the signal intensity for each lane was determined before and after denaturation using Imagequant software. The overhang intensity is determined by the ratio of the signal before and after denaturation. The relative overhang intensity is determined relative to the ratio obtained with cells infected with the empty vector (set at 100%).

Analysis of the 5′ terminal telomeric sequence

The 5′ terminal nt was assayed as described previously (Sfeir *et al*, 2005). For each DNA sample, multiple ligation reactions were performed with individual C-telorettes (see below). *Eco*RI digested genomic DNA (10 ng) was incubated in 10 µl reaction mix (1 × ligase buffer, 0.5 U T4 ligase, 10^{-2}–10^{-5} µM of individual telorettes), at 35°C for 12 h. Multiple PCR amplification reactions were performed (26 cycles of 95°C for 15 s, 58°C for 20 s, and 72°C for 10 min) using 1 U of Fail Safe enzyme mix (Epicenter), 12.5 µl Fail Safe buffer H (2 ×, manufacturer), and 0.1 µM primers (XpYp E2 forward primer and Teltail reverse primer (Baird *et al*, 2003)) in a final volume of 25 µl, containing DNA at 200 pg/µl. Amplification products were resolved on a 0.5% agarose gel, denatured, transferred onto a positively charged nylon membrane (Zetaprobe; Bio-Rad), fixed with UV, and hybridized with a subtelomeric probe (generated by PCR amplification using XpYpE2 and XpYpB2 and labeled by random priming). The membrane was exposed to

a PhosphorImager screen, and scanned on a PhosphorImager. Primers used were as follows (Sfeir *et al*, 2005):

XpYpE2 (forward primer subtelomeric):
5′-TTGTCTCAGGGTCCTAGTG-3′;
XpYpB2 (reverse primer subtelomeric):
5′-TCTGAAAGTGGACC(A/T)ATCAG-3′;
C-telorette 1: 5′-TGCTCCGTGCATCTGGCATCCCCTAAC-3′;
C-telorette 2: 5′-TGCTCCGTGCATCTGGCATCTAACCCT-3′;
C-telorette 3: 5′-TGCTCCGTGCATCTGGCATCCCTAACC-3′;
C-telorette 4: 5′-TGCTCCGTGCATCTGGCATCCTAACCC-3′;
C-telorette 5: 5′-TGCTCCGTGCATCTGGCATCAACCCTA-3′;
C-telorette 6: 5′-TGCTCCGTGCATCTGGCATCACCCTAA-3′;
C-teltail (reverse primer):
5′-TGCTCCGTGCATCTGGCATC-3′.

Supplementary data
Supplementary data are available at *The EMBO Journal* Online.

References

Bailey SM, Cornforth MN, Kurimasa A, Chen DJ, Goodwin EH (2001) Strand-specific postreplicative processing of mammalian telomeres. *Science* **293:** 2462–2465

Bailey SM, Meyne J, Chen DJ, Kurimasa A, Li GC, Lehnert BE, Goodwin EH (1999) DNA double-strand break repair proteins are required to cap the ends of mammalian chromosomes. *Proc Natl Acad Sci USA* **96:** 14899–14904

Baird DM, Rowson J, Wynford-Thomas D, Kipling D (2003) Extensive allelic variation and ultrashort telomeres in senescent human cells. *Nat Genet* **33:** 203–207

Baumann P, Cech TR (2001) Pot1, the putative telomere end-binding protein in fission yeast and humans. *Science* **292:** 1171–1175

Baumann P, Podell E, Cech TR (2002) Human pot1 (protection of telomeres) protein: cytolocalization, gene structure, and alternative splicing. *Mol Cell Biol* **22:** 8079–8087

Bianchi A, Stansel RM, Fairall L, Griffith JD, Rhodes D, de Lange T (1999) TRF1 binds a bipartite telomeric site with extreme spatial flexibility. *EMBO J* **18:** 5735–5744

Celli G, de Lange T (2005) DNA processing not required for ATM-mediated telomere damage response after TRF2 deletion. *Nat Cell Biol* (in press)

Counter CM, Avilion AA, LeFeuvre CE, Stewart NG, Greider CW, Harley CB, Bacchetti S (1992) Telomere shortening associated with chromosome instability is arrested in immortal cells which express telomerase activity. *EMBO J* **11:** 1921–1929

d'Adda di Fagagna F, Reaper PM, Clay-Farrace L, Fiegler H, Carr P, Von Zglinicki T, Saretzki G, Carter NP, Jackson SP (2003) A DNA damage checkpoint response in telomere-initiated senescence. *Nature* **426:** 194–198

de Laat WL, Appeldoorn E, Sugasawa K, Weterings E, Jaspers NG, Hoeijmakers JH (1998) DNA-binding polarity of human replication protein A positions nucleases in nucleotide excision repair. *Genes Dev* **12:** 2598–2609

de Lange T (2005) Completing the complex: telomere tally at six. *Genes Dev,* in preparation

Dimri GP, Lee X, Basile G, Acosta M, Scott G, Roskelley C, Medrano EE, Linskens M, Rubelj I, Pereira-Smith O, Peacocke M, Campisi J (1995) A biomarker that identifies senescent human cells in culture and in aging skin *in vivo. Proc Natl Acad Sci USA* **92:** 9363–9367

Garvik B, Carson M, Hartwell L (1995) Single-stranded DNA arising at telomeres in cdc13 mutants may constitute a specific signal for the RAD9 checkpoint. *Mol Cell Biol* **15:** 6128–6138

Griffith JD, Comeau L, Rosenfield S, Stansel RM, Bianchi A, Moss H, de Lange T (1999) Mammalian telomeres end in a large duplex loop. *Cell* **97:** 503–514

Hemann MT, Greider CW (1999) G-strand overhangs on telomeres in telomerase-deficient mouse cells. *Nucleic Acids Res* **27:** 3964–3969

Herbig U, Jobling WA, Chen BP, Chen DJ, Sedivy JM (2004) Telomere shortening triggers senescence of human cells through a pathway involving ATM, p53, and p21(CIP1), but not p16(INK4a). *Mol Cell* **14:** 501–513

Karlseder J, Broccoli D, Dai Y, Hardy S, de Lange T (1999) p53- and ATM-dependent apoptosis induced by telomeres lacking TRF2. *Science* **283:** 1321–1325

Kim SH, Beausejour C, Davalos AR, Kaminker P, Heo SJ, Campisi J (2004) TIN2 mediates functions of TRF2 at human telomeres. *J Biol Chem* **279:** 43799–43804

Lei M, Podell ER, Cech TR (2004) Structure of human POT1 bound to telomeric single-stranded DNA provides a model for chromosome end-protection. *Nat Struct Mol Biol* **11:** 1223–1229

Liu D, Safari A, O'Connor MS, Chan DW, Laegeler A, Qin J, Songyang Z (2004) PTOP interacts with POT1 and regulates its localization to telomeres. *Nat Cell Biol* **6:** 673–680

Loayza D, De Lange T (2003) POT1 as a terminal transducer of TRF1 telomere length control. *Nature* **424:** 1013–1018

Loayza D, Parsons H, Donigian J, Hoke K, De Lange T (2004) DNA binding features of human POT1: a nonamer 5′-TAGGGTTAG-3′ minimal binding site, sequence specificity, and internal binding to multimeric sites. *J Biol Chem* **279:** 13241–13248

Makarov VL, Hirose Y, Langmore JP (1997) Long G tails at both ends of human chromosomes suggest a C strand degradation mechanism for telomere shortening. *Cell* **88:** 657–666

Nikitina T, Woodcock CL (2004) Closed chromatin loops at the ends of chromosomes. *J Cell Biol* **166:** 161–165

Sfeir A, Chai W, Shay JW, Wright WE (2005) Telomere-end processing; the terminal nucleotides of human chromosomes. *Mol Cell* **18:** 131–138

Smogorzewska A, de Lange T (2004) Regulation of telomerase by telomeric proteins. *Ann Rev Biochem* **73:** 177–208

Smogorzewska A, Karlseder J, Holtgreve-Grez H, Jauch A, de Lange T (2002) DNA ligase IV-dependent NHEJ of deprotected mammalian telomeres in G1 and G2. *Curr Biol* **12:** 1635

Stansel RM, de Lange T, Griffith JD (2001) T-loop assembly *in vitro* involves binding of TRF2 near the 3′ telomeric overhang. *EMBO J* **20:** E5532–E5540

Takai H, Smogorzewska A, de Lange T (2003) DNA damage foci at dysfunctional telomeres. *Curr Biol* **13:** 1549–1556

van Steensel B, Smogorzewska A, de Lange T (1998) TRF2 protects human telomeres from end-to-end fusions. *Cell* **92:** 401–413

Veldman T, Etheridge KT, Counter CM (2004) Loss of hPot1 function leads to telomere instability and a cut-like phenotype. *Curr Biol* **14:** 2264–2270

Yang Q, Zheng YL, Harris CC (2005) POT1 and TRF2 cooperate to maintain telomeric integrity. *Mol Cell Biol* **25:** 1070–1080

Ye JZ, Hockemeyer D, Krutchinsky AN, Loayza D, Hooper SM, Chait BT, De Lange T (2004) POT1-interacting protein PIP1: a telomere length regulator that recruits POT1 to the TIN2/TRF1 complex. *Genes Dev* **18:** 1649–1654

Zhu XD, Niedernhofer L, Kuster B, Mann M, Hoeijmakers JH, de Lange T (2003) ERCC1/XPF removes the 3′ overhang from uncapped telomeres and represses formation of telomeric DNA-containing double minute chromosomes. *Mol Cell* **12:** 1489–1498

Supplemental Figure 1 Hockemeyer et al.

Supplemental Figure 2   Hockemeyer et al.
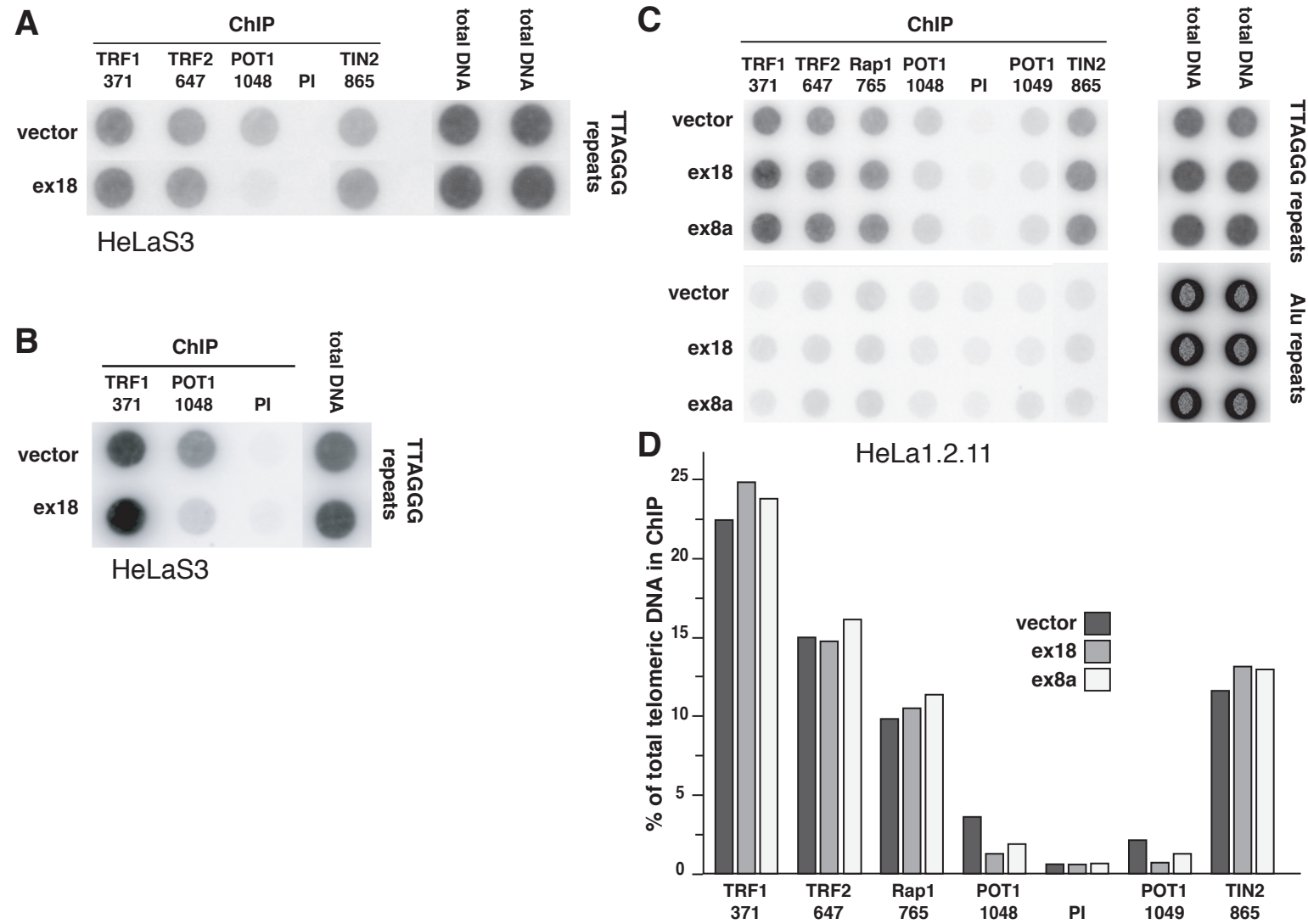
Supplemental Figure 3   Hockemeyer et al.
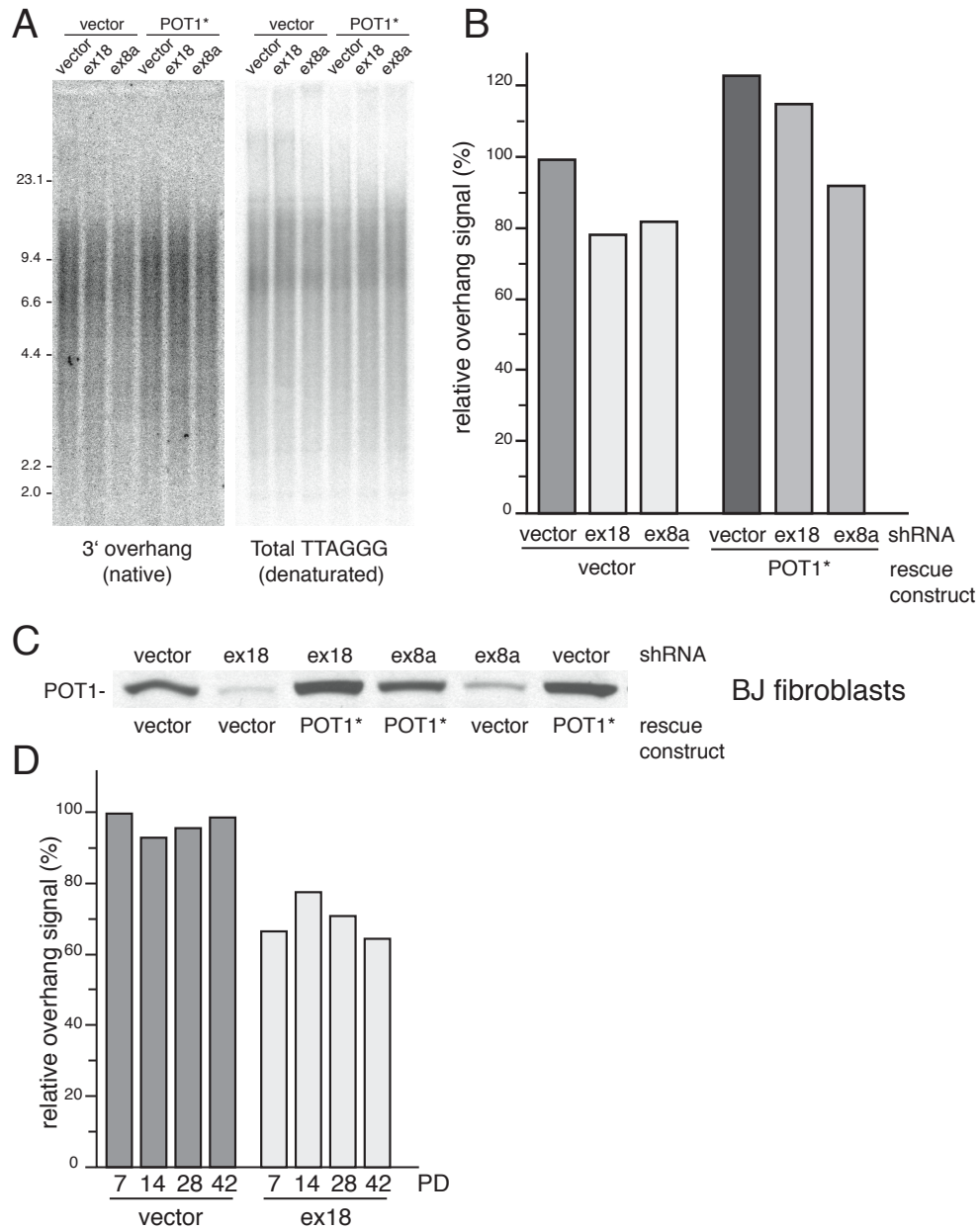
Legend to Supplemental Figures

Supplemental Figure 1.

(A) Schematic of POT1 mRNAs variant 1 and 4 and the si/shRNAs target sites used in this study.

(B) Immunoblot of HeLa cells transfected with the indicated siRNAs and BJ/hTERT cells infected with the indicated shRNA vectors. HeLa cells were analyzed 2 days (top panel) or at the indicated time points (middle panel) after transfection. BJ/hTERT cells were analyzed 5 days after infection and selection.

Supplemental Figure 2. Diminished telomeric accumulation of POT1, but not other telomeric proteins upon POT1 shRNA

(A-C) ChIPs with the indicated antibodies using HeLa cells expressing the indicated POT1 shRNAs. DNA in the IPs was dot-blotted and hybridized with a probe for telomeric DNA (from pSP73.Sty11) or Alu repeats. Total DNAs and cloned telomeric DNA (TTAGGGn) samples were blotted in parallel. Antibodies are indicated above each row. PI is pre-immuno sera from the rabbit that generated serum 1048.

(D) Bargraph of quantification of the data in (C). The reduction of POT1 at telomeres in panels (C) is less than in the other two experiments. The average reductions is ~7-fold (see text). There was no significant reduction of the accumulation of other telomeric proteins.

Supplemental Figure 3. Loss of overhang signal can be rescued by expression of full length POT1 and persists during long-term culturing.

(A) Autoradiographs of G-strand overhang assay on BJ fibroblast expressing the indicated shRNAs in combination with a version of POT1 (POT1*) that is resistant to shRNA ex18 or the empty retroviral vector. Cells were analyzed at 5 PDs after introduction of the shRNA.

(B) Bargraph representing quantified data from (A).

(C) Immunoblot of POT1 levels in the cell lines used in (A) using antibody #978.

(D) Bargraph of G-strand show the relative overhang signal in long term cultures of HeLa cells expressing the indicated shRNAs. Methods are described in (A) and (B).